Bidentate Ligation of Heme Analogues; Novel Biomimetics of the Peroxidase Active Site

Gonen Ashkenasy,[a, c] David Margulies,[a] Clifford E. Felder,[a] Abraham Shanzer,*[a] and Linda S. Powers*[b]

Abstract: The multifunctional nature of proteins that have iron–heme cofactors with noncovalent histidine linkage to the protein is controlled by the heme environment. Previous studies of these active-site structures show that the primary difference is the length of the iron-proximal histidine bond, which can be controlled by the degree of H-bonding to this histidine. Great efforts to mimic these functions with synthetic analogues have been made for more than two decades. The peroxidase models resulted in several catalytic systems capable of a large range of oxidative transformations. Most of these model systems modified the porphyrin ring covalently by directly binding auxiliary elements that control and facilitate reactivity; for example, electron-donating or -withdrawing substituents. A biomimetic approach to enzyme mimicking would have taken a different route, by attempting to keep the porphyrin ring system unaltered, as close as possible to its native form, and introducing all modifications at or close to the axial coordination sites. Such a model system would be less demanding synthetically, would make it easy to study the effect of a single structural modification, and might even provide a way to probe effects resulting from porphyrin exchange. We introduce here an alternative model system based on these principles. It consists of a two component system: a bis-imidazolyl ligand and an iron–porphyrin (readily substituted by a hemin). All modifications were introduced only to the ligand that engulfs the porphyrin and binds to the iron's fifth and sixth coordination sites. We describe the design, synthesis, and characterization of nine different model compounds with increased complexity. The primary tool for characterizing the environment of each complex Fe^{III} center was the Extended X-ray Absorption Fine Structure (EXAFS) measurements, supported by UV/Vis, IR, and NMR spectroscopy and by molecular modeling. Introduction of asymmetry, by attaching different imidazoles as head groups, led to the formation of two axial bonds of different length. Addition of H-bonds to one of the imidazoles in an advanced model increased this differentiation and expanded the porphyrin ring. These complexes were found to be almost identical in structure to peroxidase active sites. Similarly to the peroxidases and other synthetic models, these compounds stabilize the green, compound **I**-like intermediate, and catalyze the oxidation of organic substrates.

Keywords: biomimetic catalysis · heme proteins · N ligands · porphyrinoids · protein models

Introduction

Even though the globins function as oxygen-transport proteins and the peroxidases and catalases perform catalytic substrate oxidations and reductions, they share features of the heme active site: an iron-protoporphyrin IX prosthetic group that is linked to the protein by a proximal histidine residue. In peroxidases, the sixth distal position of the heme is occupied by a water molecule or by another amino acid from the protein, while globins bind small molecules like O_2 and CO. The peroxidases react with peroxide to form reactive ferryl iron intermediates—known as compounds **I** and **II**.[1, 2] Myoglobin reacts slowly with peroxide to form a myoglobin-peroxide species similar to compound **II**[3] that contains a single oxidizing equivalent above the met form. However, myoglobin uses its own amino acid side chain as a substrate; this renders it inactive after a few cycles.[4]

The primary structural difference between these active sites is the length of the iron-proximal histidine bond, which is about 0.2 Å shorter in horseradish peroxidase and cytochrome C peroxidase than in myoglobin or hemoglobin.[5–12] Studies have shown that strong hydrogen bonding to the

[a] Prof. Dr. A. Shanzer, Dr. G. Ashkenasy, D. Margulies, Dr. C. E. Felder
Department of Organic Chemistry
The Weizmann Institute of Science, Rehovot, 76100 (Israel)
Fax: (+972) 89342917
E-mail: coshanzr@wicc.weizmann.ac.il

[b] Prof. Dr. L. S. Powers
National Center for the Design of Molecular Function
Utah State University, Logan, Utah 84322-4155 (USA)

[c] Dr. G. Ashkenasy
Present address: The Scripps Research Institute
La Jolla, California (USA)

  0947-6539/02/0817-4017 $ 20.00+.50/0

proximal histidine in the peroxidases—for example, in cytochrome C peroxidase these H-bonds are formed by His175, Asp235, and Trp191—results in an increased electron density on the heme active site; this stabilizes both the iron and radical electron-deficient centers that exist in the catalytic intermediates.[13–17] This strong H-bonding has also been shown by Powers and co-workers, using site-specific mutagenesis studies, to be responsible for the shorter iron-proximal histidine–nitrogen ($Fe-N_{\varepsilon}$) bond.[9, 11, 12]

During the last two decades, several research groups have manipulated the structure of metalloporphyrin complexes in order to mimic the peroxidatic activity. Valentine, Groves, Dolphin, Traylor, Mansuy, their co-workers, and others have extensively studied models that utilized the Fe^{III} and Mn^{III} complexes of *meso*-tetramesityl porphyrin (TMP) or of halogenated porphyrins. These molecules prevent the formation of unreactive μ-oxo dimmers and self-oxidation of the porphyrin. Thus, they enable the formation of compound **I**- or **II**-like intermediates and catalyze the oxidation of alkenes, alkanes, and other substrates.[18–25] In such model systems, as in the enzymes, the catalytic process is enhanced with respect to rate and yield once the fifth metalloporphyrin coordination site is ligated by a nitrogen-containing ligand, generally an imidazole.[20, 22] The effect of hydrogen bonding to this imidazole on reactivity has only been sporadically investigated.[18, 20, 22, 26] We note the recent contribution of Nakamura and co-workers that probed the effect of hydrogen bonding in thiolated ligands on the structure and reactivity of cytochrome P450 models,[27, 28] and of Nocera and co-workers that demonstrated the ability to orient exogenous water next to the metal center by hydrogen bonding.[29]

In almost all of the structures studied—and the same is true for models of cytochrome P450—the auxiliary elements that control and facilitate reactivity were attached to the porphyrin ring *covalently*. However, a biomimetic approach would follow the evolutionary process, attempting to keep the porphyrin ring system unaltered, as close as possible to its native form, and introduce all modifications at or close to the axial coordination sites. Such an approach is less demanding synthetically, because chemical transformations are performed on an alkyl (or peptide) chain rather than on the porphyrin aromatic ring. It supplies a convenient platform from which to probe the effect of a single modification on the structure and reactivity of the entire complex. In addition, it allows the easy exchange of the iron–porphyrin for another metalloporphyrin.

Recently, we reported the characterization of metalloporphyrin complexes with the dipodal ligands **1** and **2** (Scheme 1), for the development of NO sensors.[30] These ligands posses two arms that wrap around metalloporphyrin moieties and bind to the metal center. The complexes bind to solid surfaces through the ligand disulfide rings and form well-defined monolayers. These monolayers on a GaAs surface bind NO, and detection of the binding event is achieved by tracking changes in the surface electronic properties. It occurred to us that the skeletons of ligands **1** and **2** might serve as a platform for the incorporation of auxiliary groups that will provide an array of complexes with metalloporphyrins that will mimic the peroxidase active site.

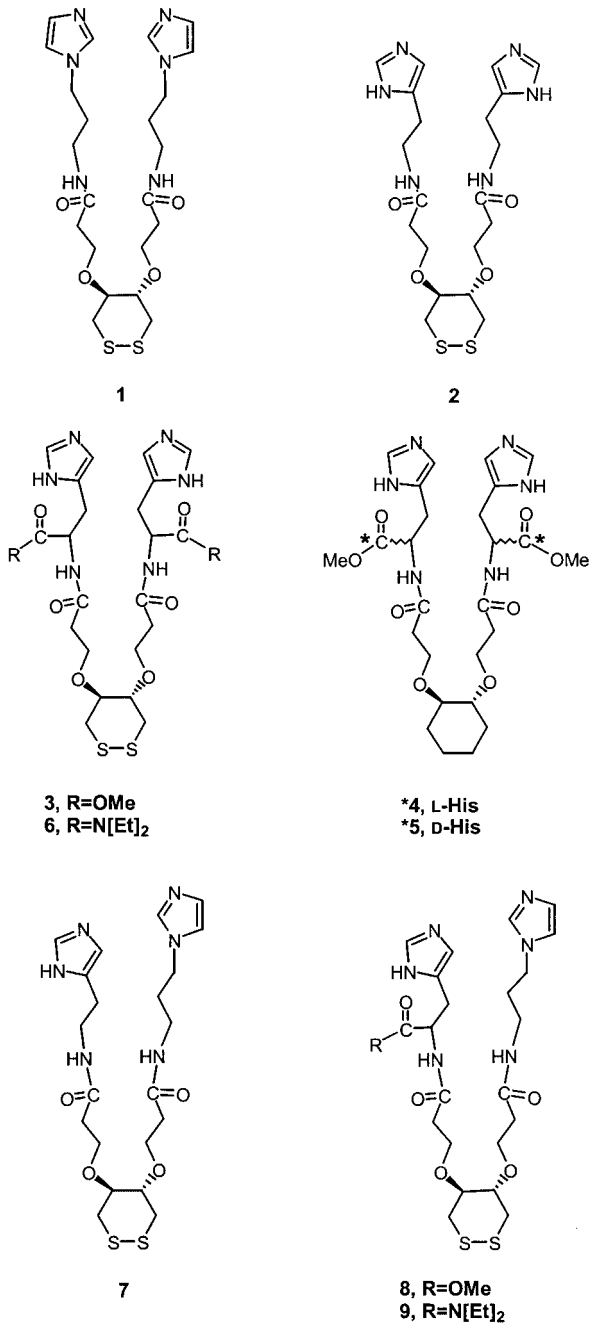

Scheme 1. Bidentate ligands. **1** and **2**: symmetric "parent" ligands, **3**–**6**: symmetric ligands with H-bonding between the side-chain carbonyl and the imidazole head group, **7**: asymmetric ligand, **8** and **9**: asymmetric ligands with a single H-bond to the NH-imidazole.

We describe here the design, synthesis, and characterization of a novel set of complexes made from the organic tailor-made ligands **1**–**9** (Scheme 1) and iron(III) porphyrins. All variations between complexes were introduced only onto the ligand that engulfs the heme and binds to the iron fifth and sixth coordination sites, while the Fe^{III} porphyrins, FeTPPCl (TPP = tetraphenylporphyrin) and FeDMPPCl (DMPP = dimethyl ester of protoporphyrin IX), were utilized without altering their porphyrin skeleton. The parent ligands, **1** and **2**, were first modified by breaking the symmetry of the ligand in such a way as to guarantee differentiation between the two

0947-6539/02/0817-4018 $ 20.00+.50/0 *Chem. Eur. J.* **2002**, *8*, No. 17

axial bond lengths. We then introduced a selective hydrogen bond to only one of the imidazole groups in order to mimic the extensive hydrogen-bonding network observed in peroxidases. UV/Vis titrations, and electron spray MS and ^{1}H NMR spectroscopy measurements showed the formation of the desired 1:1 ligand-to-Fe^{III} porphyrin complexes. The environment of the complex Fe^{III} center was characterized thoroughly with Extended X-ray Absorption Fine Structure (EXAFS) measurements, and the results were supported by spectroscopic (UV/Vis, IR, and NMR) and theoretical (EFF calculations) tools. The first-coordination-shell bond lengths in the more advanced complexes, made of ligands **7**–**9** in Scheme 1, were found to be practically identical to those in the active sites of horseradish peroxidase, cytochrome C peroxidase, *Arthromyces ramosus* peroxidase, and myeloperoxidase. Similarly to the peroxidases and other synthetic models, these biomimetic compounds stabilize the green oxoferryl-porphyrin radical cation and catalyze the oxidation of organic substrates.

Experimental Section

Synthesis: The synthesis of the active-ester precursor **I** (Scheme 2) was described earlier.[31]

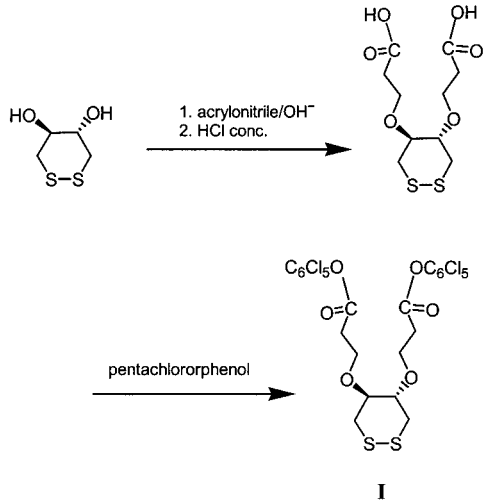

I

Scheme 2. Synthesis of the precursor **I**.

*Preparation of the symmetric ligands **1**–**3** and **6***: The appropriate amino imidazole (2.0 mol equiv.) and triethylamine (2.0 equiv) were added to a solution of **I** (1.0 equiv) in $CHCl_3$ or THF, and the reaction mixture was stirred at room temperature overnight. The solvent was removed and the product was separated on a silica column ($CHCl_3/CH_3OH$, 8:2, 50–70% yields). Compound **3:** IR (KBr) $\tilde{\nu}=1099$ (ether), 1650 (CONH), 1739 (COOMe); ^{1}H NMR (400 MHz, CD_3OD) $\delta=7.58$ (s, 2H), 6.87 (s, 2H), 4.67 (m, 2H), 3.75 (m, 4H), 3.68 (s, 6H), 3.20 (m, 2H), 2.90–3.15 (br, 2H + 4H), 2.65 (m, 2H), 2.43 (m, 4H). Compound **6:** IR (KBr) $\tilde{\nu}=1102$ (ether), 1633 (CON-Et$_2$), 1652 (CONR); ^{1}H NMR (400 MHz, CD_3OD) $\delta=7.61$ (s, 2H), 6.87 (s, 2H), 5.07 (t, $J=7.0$ Hz, 2H), 3.78 (m, 4H), 3.45 (m, 4H + 2H), 3.20 (m, 4H), 2.95 (m, 4H), 2.70 (m, 2H), 2.44 (m, 4H), 1.14 (t, $J=6.5$ Hz, 6H), 1.06 (t, $J=6.5$ Hz, 6H). MS (ES) $m/z=681$ [M^++H]. The spectral characterizations of ligands **1** and **2** have been published before.[30]

*Preparation of ligands **4** and **5***: The enantiomerically pure cyclohexyl derivative of **I** was prepared in a similar fashion to **I** from (1S,2S)-*trans*-1,2-cyclohexanediol (Sigma), and was used as a precursor for the synthesis of ligands **4** and **5**. The two different diastereomers were prepared by coupling this active ester to 2.0 mol equiv. of L-histidine methyl ester (**4**), or D-histidine methyl ester (**5**), in the same procedure as described above for **3**. Compound **4:** ^{1}H NMR (400 MHz, CD_3OD) $\delta=7.63$ (s, 2H), 6.90 (s, 2H), 4.70 (m, 2H), 3.77 (m, 4H), 3.70 (s, 6H), 3.12 (m, 4H), 3.08 (m, 2H), 2.46 (t, $J=6.2$ Hz, 4H), 1.96 (br, 2H), 1.61 (br, 2H), 1.18 (m, 4H). Compound **5:** ^{1}H NMR (400 MHz, CD_3OD) $\delta=7.62$ (s, 2H), 6.88 (s, 2H), 4.70 (m, 2H), 3.75 (m, 4H), 3.69 (s, 3H), 3.12 (m, 4H), 3.01 (m, 2H), 2.44 (m, 4H), 1.95 (br, 2H), 1.82 (br, 2H), 1.18 (m, 4H).

*Preparation of the nonsymmetric ligands **7**–**9***: 1-(3-Aminopropyl)-imidazole (0.9 mol equiv.) and triethylamine (0.9 equiv.) were added to a solution of **I** (1.0 equiv.) in THF, and the reaction mixture was stirred at room temperature, until all the amine was consumed (tlc). The appropriate amino NH-imidazole (1.2 equiv.) and triethylamine (1.2 equiv.) were added, and the mixture was stirred overnight. The solvent was removed, and the nonsymmetric compound was separated from the two symmetric compounds over a silica column ($CHCl_3/CH_3OH/NH_3$, 8:2:drops). The detailed characterization of **7** has been published recently.[32] Compound **8:** IR (KBr) $\tilde{\nu}=1100$ (ether), 1650 (CONH), 1738 (COOMe); ^{1}H NMR (400 MHz, $CDCl_3/CD_3OD$) $\delta=7.70$ (s, 1H), 7.58 (s, 1H), 7.12 (s, 1H), 6.96 (s, 1H), 6.85 (s, 1H), 4.65 (m, 1H), 4.05 (t, $J=7.2$ Hz, 2H), 3.74 (m, 4H), 3.65 (s, 3H), 3.24 (m, 2H), 3.13 (m, 2H), 3.07 (m, 2H), 2.95 (m, 2H), 2.68 (m, 2H), 2.33 (m, 4H), 1.95 (quint, $J=7.2$ Hz, 2H). Compound **9:** IR (KBr) $\tilde{\nu}=1102$ (ether), 1633 (CON-Et$_2$), 1647–1652 (CONR); ^{1}H NMR (400 MHz, CD_3OD) $\delta=7.68$ (s, 1H), 7.60 (s, 1H), 7.12 (s, 1H), 6.96 (s, 1H), 6.85 (s, 1H), 5.06 (m, 1H), 4.03 (t, $J=7.2$ Hz, 2H), 3.80 (m, 4H), 3.38 (m, 4H), 3.17 (br, 4H), 2.93 (m, 2H), 2.72 (m, 2H), 2.41 (m, 2H), 1.96 (quint, $J=7.2$ Hz, 2H), 1.12 (t, $J=6.5$ Hz, 3H), 1.04 (t, $J=6.5$ Hz, 3H). MS (ES) $m/z=596$ [M^++H]. Ligands **7**–**9** were additionally characterized by 2D COSY ^{1}H NMR to ensure connectivity between the fragments of each arm.

Spectroscopic measurements

X-ray absorption spectroscopy: X-ray absorption measurements were performed at the National Synchrotron Light Source on Beamline X-9 using Si(111) crystals, which provide ≈2 eV resolution at 7 keV. Complexes and model compounds were prepared from solutions in DMF (15 mM), except for **9**-FeDMPPCl, which was found to be less soluble and was prepared from a solution of FeDMPPCl (5 mM) and excess **9** at room temperature. Then, the samples were frozen and maintained at ≈ −80 °C during X-ray exposure to minimize radiation damage.[33]

Data were analyzed according to previously described methods[5–12, 34–40] as well as by using the UWXAFS package.[41] A considerable number of crystallography studies on heme proteins and model compounds have shown that the largest differences/changes in bond lengths occur in the first coordination shell. Thus, our analyses concentrate on the first coordination shell.

Briefly, the absorption below the edge was set equal to zero. The EXAFS modulations were isolated by background subtraction and normalization, k^3-multiplication, which approximately equalizes the modulations in k-space (k is the wave vector, Figure 1a), and Fourier transformation, which

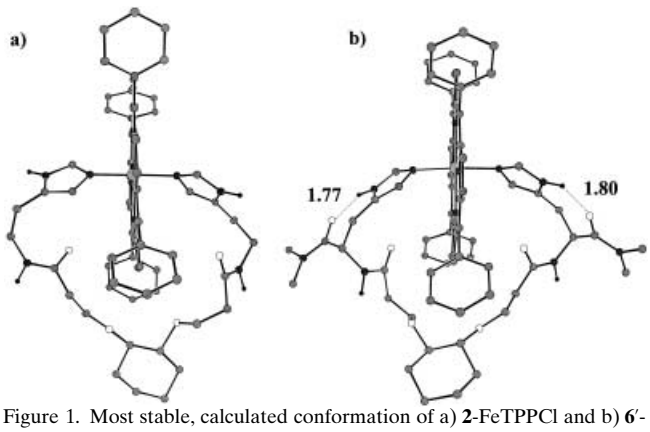

Figure 1. Most stable, calculated conformation of a) **2**-FeTPPCl and b) **6′**-FeTPPCl. The view is almost along the porphyrin plane, the two imidazoles are in the center left and right, bound to the central iron atom, and the anchor base is at the bottom. The H-bonds in **6′**-FeTPPCl are shown as dashed lines, with the lengths indicated [Å]. Atom coding: lightly shaded: carbon, darkly shaded: nitrogen, black: hydrogen, and white: oxygen. Most of the hydrogens are not shown for clarity, but were included in the calculation.

  0947-6539/02/0817-4019 $ 20.00+.50/0

converts the data to distance space (Figure 1b). The contribution of each shell was isolated by application of a Fourier window filter and back-transformation, or the background was subtracted, k^3-multiplied data can be used directly. Thus, for each coordination shell, the amplitude contains the number of scattering atoms [N] and their Debye–Waller factors [σ^2], while the phase contains the average length [r] and the threshold energy [E_o]. Comparison of the sample amplitude and phase with those of carefully chosen model compounds having similar structure and for which the structure has been determined gives the sample parameters: r, N, $\Delta\sigma^2$, and ΔE_o, where Δ = (model-protein). The goodness of fit was judged by the sum of the residuals squared, ΣR^2. Results of the fitting procedures were compared by using the statistical arguments of Powers and Kincaid.[37]

For a solution to considered "best", it must satisfy the following criteria: i) all parameters must be physically reasonable, ii) the sum of the residuals squared must be smaller than all other physically reasonable solutions by at least a factor of 1.4, iii) all distance parameters of one solution must differ from those of another solution by at least their respective estimated errors, and iv) the residuals must be comparable to the total error in the data. In order to demonstrate that these methods are capable of resolving the reported lengths in the data, data having the same parameters as those found for the experimental data were synthesized by using the amplitudes and phases from model compounds. Gaussian noise was added in the amount contained in the experimental data, and these synthetic data were then analyzed. Lengths like those reported for the experimental data can clearly be reliably distinguished.[37]

Optical absorption spectroscopy (UV/Vis): All measurements were made on a Beckman DU-7500 diode-array spectrophotometer. Typical spectra of the Fe^{III}–porphyrin complexes (22 °C, 1×10^{-5}–5×10^{-4} M, DMF or $CHCl_3$) were found to be as follows, FeTPPCl + **1**–**6**: λ = 416–419 nm ($\varepsilon\approx150\,000$), 550–551 (9000); **7**-FeTPPCl λ = 416 nm ($\varepsilon\approx150\,000$), 541 (9000); **9**-FeTPPCl λ = 406 nm ($\varepsilon\approx130\,000$), 525 (br, $\varepsilon\approx5000$); FeDMPPCl + **1**–**6**: λ = 412–414 nm ($\varepsilon\approx150\,000$), 534–539 (13 500). Fe^{III}–porphyrins titrations with increasing amounts of the ligands (**1**–**3**) were monitored at room temperature, and the changes in the spectra relative to the free-base Fe^{III}–porphyrin were utilized to calculate the binding constants (K_1 and β_2) of the bis-imidazolyl binding sites to the central metal ions, similarly to the way described in Walker et al.[42] Experiments to follow the oxidation of the complexes to the ferryl radical cation were made in isolated and cooled UV/Vis cells.

Electron spray MS: Samples obtained from the ligand-to-Fe^{III}–porphyrin solutions (1:1, 15 mM in $CHCl_3$ or $CHCl_3/CH_3OH$ 8:2) were analyzed by ES-MS, and the detector was set to look for these species as well as for higher-order oligomers. The molecular mass of the cationic complex without the chlorine counter ion is generally observed, together with the Na^+ adduct, and in some cases with a small amount of the free ligand. The following m/z values were observed for complexes of the symmetric ligands with FeTPPCl: [**1**-FeTPP]$^+$: 1178 [M^++H], 511 [**1**$^+$+H]; [**2**-FeTPPCl]$^+$: 1150 [M^++H], 483 [**2**$^+$+H]; **3**-FeTPPCl: 1267 [M^++H], 598 [**3**$^+$+H]; [**6**-FeTPPCl]$^+$: 1350 [M^++H], 1373 [M^++H+Na^+].

NMR measurements: ^{1}H NMR measurements of the complexes were carried out on a Bruker AMX-400 spectrometer. The samples of low-spin ligand-to-Fe^{3+}–porphyrin solutions (1:1, 22–25 mM in $CDCl_3$, $CDCl_3$/CH_3OH 8:2, or [D_7]DMF) were measured at different temperatures (−40 to +50 ± 0.1 °C). All chemical shifts are reported in δ units from TMS as internal standard. The oxidation products in [D_7]DMF were followed at low temperatures (< −30 °C), and the decomposition of these species was monitored by slowly heating the sample to above −5 °C in the NMR machine.

Molecular modeling: Molecular-mechanics calculations of **2**-FeTTPCl, **3**-FeTPPCl, and a complex equivalent of **6**-FeTPPCl (having dimethyl amide side chains), in which the disulfide bases were replaced by cyclohexyls, were done by using the locally developed EFF force field.[32] The partial atomic charges on the imidazole moieties were adjusted with the help of MOPAC and of DFT calculations[43] on an imidazole, both isolated and complexed with Zn^{+2} or NH_4^+, respectively. These calculations showed that the imidazole ring becomes substantially more positively charged upon complexation. The final values used were: N1 (bound to the Fe^{3+}) −0.89, C2 and C5 0.0, H on C2 or C5 +0.11, N3 +0.11, H on N3 +0.42, C4 +0.03, and +0.11 was added to the carbon of the first side-chain methylene.

Oxidation reactions

Oxoferryl radicals. Complexes of the bis-imidazole ligands with FeTPPCl (in DMF or $CHCl_3/CH_3OH$ 8:2) were prepared at room temperature in concentration ranges that ensured complete binding (> 99 %). The solution was then cooled (−78 < T < −20 °C), and the oxidant *meta*-chloroperbenzoic acid (*m*CPBA, 5–10 mol equiv.) was added in one aliquot. The reactive species was formed over several minutes at moderately low temperatures (≈ −30 °C), and much more slowly at −78 °C. Fast regeneration of the low-spin Fe^{III} complexes was evidenced after heating the solution (T > −5 °C), or after addition of cyclooctene (5 mol equiv.) to the cold solution.

Oxidation of ABTS: A solution of ABTS (2,2′-azino-di-(3-ethylbenzthiazoline-6-sulphonic acid), Sigma, 4.0×10^{-5} M), containing complexes of the bis-imidazole ligands (8 mM) and FeTPPCl (1.3×10^{-5} M) in DMF (200 μL) at 22 °C was titrated by stepwise addition of *m*CPBA aliquots (80 mol equiv.). When equilibrium had been reached, a wavelength scan of the cuvette was obtained and was interpreted for the ratio between the starting material ABTS and its radical cation.[44] Ten to twelve portions were sufficient to obtain a stable, exclusive spectrum of the product. In the kinetic experiments, the spectral changes of the initial oxidation steps were followed, every 0.1–0.3 seconds, immediately after the addition of the first *m*CPBA portion. To compare the reactivity of the three complexes, **2**-, **7**-, and **9**-FeTPPCl, we performed several sets of experiments in triplicate, in which identical conditions of temperature, concentration, total solution volume, and stirring were maintained. All three reactions appeared to follow second-order kinetics, first-order with respect to the catalyst and ABTS concentrations.

Results and Discussion

Design and synthesis

Ligands: All together, nine bis-imidazolyl ligands, shown in Scheme 1, were synthesized by using a procedure similar to that described earlier for ligands **1** and **2**.[30] In the final step, the dipentachloro phenolate **I**, synthesized as described in Scheme 2, was coupled to the appropriate amine(s) in order to obtain the individual derivative. Ligands **1** and **2** consist of two alkyl chains with *N*-alkyl (**1**) or NH (**2**) imidazoles as head groups for intramolecular, unstrained binding of metalloporphyrins. Ligands **3** and **6** are modified versions of **2**, made of L-histidine derivatives. These compounds posses carbonyl groups at the side chains that can form seven membered rings in aprotic solvents through intramolecular hydrogen bonding to the NH groups of their imidazoles. Ligands **4** and **5** are similar to **3**, but have cyclohexyl as bases and are diastereomerically pure. These were made as controls to demonstrate that the utilization of disulfides and/or racemic mixtures produces no observable differences.

The asymmetric ligand **7** has one *N*-alkyl imidazole (as in ligand **1**) and one NH imidazole (as in **2**) on the same skeleton. NH imidazoles bind iron–porphyrins much more strongly than *N*-alkyl imidazoles,[42] thus this ligand was designed to form complexes with one short and one longer axial bond to the central Fe^{III} ion. The structures of **8** and **9** contain both features described above. These ligands have NH and *N*-alkyl imidazoles to create nonsymmetric binding to iron–porphyrins, and a carbonyl at one side chain for H-bonding only to the imidazole NH. All ligands were placed on top of a cyclic disulfide ring that provides the means for future anchoring to solid support.[30]

0947-6539/02/0817-4020 $ 20.00+.50/0 *Chem. Eur. J.* **2002**, *8*, No. 17

Iron–porphyrin complexes: Complexes of the ligands with metalloporphyrins were prepared either by adding an excess of the ligand to a dilute solution ($1\times10^{-5}-5\times10^{-4}$ M) of Fe^{III}–porphyrins or by simple mixing of equimolar concentrated solutions ($c=15$ mM, $CHCl_3$ or DMF). In the first method, titrations of Fe^{III}–porphyrins with the symmetric ligands **1**–**3** were monitored by UV/Vis measurements, and changes in the spectra relative to the free-base metalloporphyrins were utilized to calculate the binding constants (K_1 and β_2) of the bis-imidazolyl binding sites to the central metal ions.[42] The representative reaction (1) reflects the desired stoichiometry when both imidazoles (Im) of a single ligand bind to the metalloporphyrin. An equivalent equation can be derived to show the step-by-step binding of the two imidazolyl fragments, and thus to reveal the relative stability of the monoligated complex by using K_1. The formation constants obtained from the titrations with these ligands, as well as with their single-stranded analogues, are summarized in Table 1—the β_2 values fall in the range of 10^3-10^4 M^{-2}.

$$FeTPPCl + 2\,Im \overset{\beta_2}{\rightleftharpoons} FeTPPCl(Im)_2{}^+Cl^- \quad (1)$$

Table 1. Formation constants for ligand–Fe^{III}-porphyrin complexes.

Metalloporphyrin	Ligand	Solvent	K_1 [M^{-1}]	$\beta_2\times10^{-4}$ [M^{-2}][a]
FeTPPCl	**1**	DMF		1.1
	AcPrIm[b]	DMF	≈50	0.4
	2	DMF		2.2
	A-His[b]	DMF		1.3
	3	DMF		2.3
FeDMPPCl	**1**	$CHCl_3$		2.4

[a] Calculated with respect to concentrations of imidazolyl residues. [b] AcPrIm = *N*-acetyl-1-(3-aminopropyl) imidazole, A-His = *Nω*-acetyl-histamine.

Inspection of Table 1 reveals higher β_2 values for the dipodal ligands (**1** and **2**) relative to their single-stranded model compounds (AcPrIm and A-His, respectively). Titration of FeTPPCl with the symmetric dipodal ligands showed no formation of a monoimidazolyl complex, although such intermediates were observed with the single-stranded models AcPrIm (Table 1, $K_1\approx50\,M^{-1}$) and with *N*-methyl imidazol.[42] These results demonstrate not only the well-known formation of diimidazolyl complexes with iron–porphyrins, but also the strong tendency of the dipodal ligands to undergo intramolecular reactions, to form complexes of 1:1 stoichiometry (chelation effect). The exclusive formation of complexes with such a stoichiometry was also evidenced by ES-MS analysis of the complexes; this showed that the 1:1 cationic complexes (without the Cl^-) gave rise to the major peak, and no oligomers of higher mass (see Experimental Section for m/z values).

The moderate formation constants (β_2) in Table 1 correlate excellently with stability-constant values obtained earlier for complexes of substituted imidazols and metalloporphyrins.[42] A simple calculation revealed that these complexes are the dominant species when solutions of 10^{-3} M concentration or higher are utilized. Indeed, all other experiments described here (FTIR, NMR, EXAFS etc.), were performed with complexes that were synthesized by the second method ($c=15$ mM), in which more than 99% of the molecules are in the bis-imidazolyl complex form.

^{1}H NMR measurements of each low-spin complex of the Fe^{III}–porphyrins FeDMPPCl and FeTPPCl with the ligands, which were obtained by using the second-complexation method, yielded spectra that belong to only a single species. All the proton chemical shifts could be assigned by following the changes with temperature in the spectra of FeTPPCl complexes with the symmetric ligands (**1**, **2, 3** or **6**) because of simplification owing to their C_2 symmetry. Complexes of FeDMPPCl were compared to previously reported systems in order to resolve the chemical shifts in the high ($\delta<0$) and low ($\delta>10$ ppm) field spectra.[45] Interestingly, for the spectrum of the nonsymmetric complex **7**-FeTPPCl, one can also assign the peaks of protons in the vicinity of the paramagnetic center. Different chemical shifts were observed for the two C2-bound imidazole protons ($\delta=-7.8$ and -15.6 ppm, [D_7]DMF, 240 K) and for the CH_2-imidazole protons ($\delta=17.9$ and 19.2 ppm), which are located on opposite arms of the ligand.

Molecular mechanics were used to determine the lowest-energy conformations of **2**-FeTPPCl, **3**-FeTPPCl, and **6′**-FeTPPCl (a complex possessing dimethyl amide side chains, equivalent to **6**-FeTPPCl). The S–S bond in each ligand was replaced by a C–C bond. The structures obtained, as shown in Figure 1 for the most-stable conformations of **2**-FeTPPCl and **6′**-FeTPPCl, share the following features: i) the ligand strands are located above the porphyrin pyrroles, on opposite faces, between two phenyl substituents, and ii) the coordination of imidazoles to the iron center is almost perfectly axial; this gives octahedral coordination geometry.

All the stable conformations obtained for the structures of **3**-FeTPPCl and **6′**-FeTPPCl had the carbonyl side chains pointing toward the imidazole NH to form reasonably stable seven-member rings through hydrogen bonding. The H-bond lengths in the stable conformations of **6′**-FeTPPCl were found to be around 1.80 Å (Figure 1), while those in **3**-FeTPPCl are slightly longer, ≈1.95 Å.

The hydrogen bonding from the side-chain carbonyl to the imidazole NH was directly evidenced in the infrared spectra (KBr) of ligand **6** and complex **6**-FeTPPCl. The diethyl amide carbonyls on the side chains of these molecules vibrate at 1633 cm^{-1}. Exactly this value, red-shifted relative to non-associated amide carbonyls, was reported for other intramolecularly H-bonded diethyl amides.[46] The carbonyl vibrations at the ester side chains of ligand **3** and its complexes are less sensitive to association and were only slightly shifted (1738 cm^{-1}, ≈7 cm^{-1} to the red) relative to the free esters. ^{1}H NMR measurements at various temperatures (243–295 K) revealed that chemical shifts of the imidazolyl and CH_2 imidazolyl protons in **3**- and **6**-FeTPPCl are less sensitive to temperature changes than these protons in **2**-FeTPPCl. This observation is attributed to the more rigid structures that are formed in the former complexes, through hydrogen bonds that "hold" the imidazoles and side-chains together.

Ligation of the central Fe^{III} ion: Figure 2 shows the k^3-multiplied, background-subtracted, EXAFS data (A) for

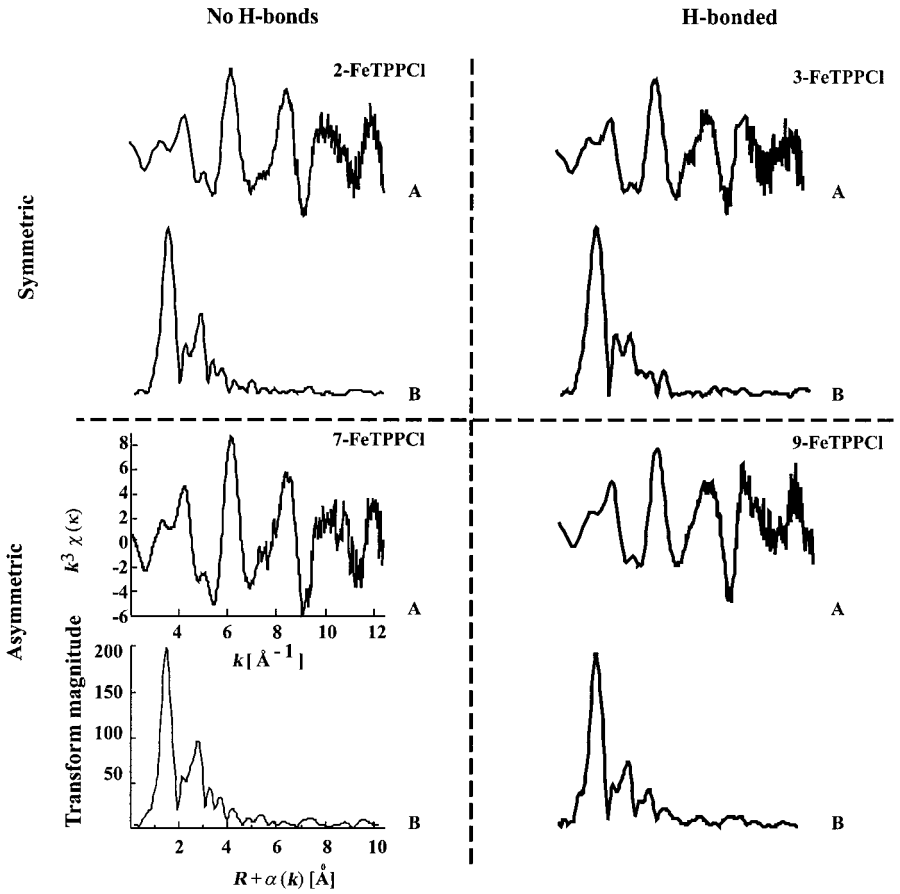

Figure 2. A) Background-subtracted, k^3-multiplied EXAFS data normalized for one absorbing atom for selected complexes formed by each type of bis-imidazole ligand and iron–porphyrin FeTPPCl. B) Fourier transform spectra of the EXAFS data in (A).

selected complexes formed by the bis-imidazole ligands and iron–porphyrin, and the Fourier transforms of this data (B). All measurements were recorded under practically identical conditions with respect to solvent (DMF), concentration ($\approx$15 mM), and temperature. The fitting results were similar to other synthetic heme compounds for which crystallography data are available.

Symmetric ligation: The first-coordination-shell bond lengths around the central iron ion for complexes of the Fe^{III}–porphyrins with the symmetric ligands **1**–**3** and **6** are compared in Table 2. The average Fe–N$_p$ bond lengths are shorter in complexes of **1** or **2** than in complexes of **3** or **6**, into which carbonyl side chains had been introduced. The axial bonds (Fe–N$_{im}$) are also longer for complexes of **3** or **6**, relative to those of **1** or **2**, but differences are smaller. The bond lengths in complexes **4**-FeDMPPCl and **5**-FeDMPPCl were found to be essentially identical ($\pm$0.01 Å) to those of **3**-FeDMPPCl. This result supports the assumption that the environment of the heme is very similar for each of the diastereomers (e.g. of **3**-FeDMPPCl), and that the disulfide base does not interfere with the iron complexation.

The elongation of the Fe–N bonds in complexes of **3**–**6** is explained by the increased electron density on the Fe^{III} due to the hydrogen bonding between the carbonyls on the ligand side chains and the free NHs of the imidazole head groups.[11, 47] The effect of hydrogen bonding was also clearly seen in the UV/Vis and ^{1}H NMR measurements. The UV/Vis spectra of **3**- and **6**-FeDMPPCl are red-shifted by 1 nm in the Soret region and by 3–5 nm in the Q-region relative to those of **1**- and **2**-FeDMPPCl. In agreement with the EXAFS results, these red shifts reflect the fact that the central Fe^{III} ions in **3**- and **6**-FeDMPPCl are axially coordinated by more electron-rich imidazoles.

Table 2 shows that slightly longer Fe–N$_p$ bonds were found for the complexes of Fe-DMPPCl with **1** or **2** (2.04 Å) than for the complexes of FeTPPCl with these ligands (2.01–2.02 Å). We attribute this difference to H-bonding from the DMPP methyl esters to one of the ligand imidazoles. This structural feature has been shown by molecular modeling in the structure of **2**-Fe-DMPPCl[32] and in the crystal structure of bis-imidazole hemin.

The bond elongation around the Fe^{III} center due to H-bonding, as evidenced also from Table 2 (**2**-FeTPPCl and **3**-FeTPPCl), is similar in magnitude to that due to the introduction of electron-donating groups on the porphyrin periphery, as seen by comparing **2**-FeTPPCl to **2**-FeTmPPCl (TmPP = tetra-*p*-methoxyphenyl porphyrin). Moreover, a large increase of the Fe^{III} first-coordination-shell bond lengths

Table 2. First-coordination-shell bond lengths [Å] for complexes of Fe^{III} porphyrins and symmetric ligands.[a]

Porphyrin	Bond	Ligand			
		1	**2**	**3**	**6**
FeTPPCl	Fe–N$_p$	2.01	2.02	2.06	2.09
	Fe–N$_{im}$	1.91	1.90	1.92	1.95
	Fe–$\bar{N}$	2.00	2.00	2.01	2.05
FeDMPPCl	Fe–N$_p$	2.04	2.04	2.07	2.08
	Fe–N$_{im}$	1.90	1.91	1.94	1.92
	Fe–$\bar{N}$	2.02	2.02	2.03	2.08
FeTmPPCl	Fe–N$_p$		2.05	2.13	
	Fe–N$_{im}$		1.95	1.99	
	Fe–$\bar{N}$		2.02	2.06	

[a] Fe–N$_p$ = Fe to N(pyrrole) average length, Fe–N$_{im}$ = Fe to N(imidazole) average length, Fe–$\bar{N}$ = Fe to N(all) average length. Error in all cases = $\pm$0.015 Å.

0947-6539/02/0817-4022 $ 20.00+.50/0 *Chem. Eur. J.* **2002**, *8*, No. 17

is found on forming the complex **3**-FeTmPPCl, in which the ligand forms H-bonds and the porphyrin contains the four methoxy electron-donating groups.

Nonsymmetric axial ligation: The EXAFS results for complexes of ligands **7**–**9** show that the data can only be adequately modeled with three atom types (e.g. for **7**-FeDMPPCl in Table 3). This indicates nonsymmetric axial ligation, which is shown schematically in Scheme 3 as Fe–N_{im} and Fe-X, respectively.

The bond lengths to Fe^{III} in complexes of **7**–**9** are summarized in Table 4. The shorter bonds (Fe–N_{im}) in complexes of ligand **7** were found to be about 1.90 Å, very similar to the Fe–N_{im} bonds in complexes of the symmetric ligand **2** (Table 2). On the other hand, the bonds to the *N*-alkyl imidazoles (Fe–X) in these complexes are significantly longer, >2.10 Å; this demonstrates nonsymmetric heme axial ligation with this simple ligand. The Q-band peak in the UV/Vis spectrum of **7**-FeTPPCl was observed at 541 nm, shifted to the blue by about 10 nm relative to the typical peak of a symmetric compound. This shift reflects the formation of an imperfect octahedral complex, in which one (nitrogen) ligand is bound weekly. As noted in the design and synthesis section, the ^{1}H NMR spectrum of **7**-FeTPPCl also showed different binding of the *N*-alkyl imidazolyl and NH imidazolyl to the central Fe^{III}.

Table 3. Fitting results for the first coordination shell of **7**-FeDMPPCl complex.

r [Å]	N	$\Delta\sigma^2$ [Å^2][a]	ΔE_0 [eV][b]	ΣR^2
2.03[c]	4	3.7×10^{-3}	−0.4	0.7
1.87[d]	1	4.3×10^{-3}	5.1	
2.20[e]	1	4.3×10^{-3}	−1.7	
2.05	5	-1.3×10^{-3}	−1.6	5.0
2.25	1	-3.5×10^{-3}	0	
2.04	5	-7.3×10^{-4}	−0.6	3.0
1.85	1	1.9×10^{-5}	−5.1	
2.05	4.3	-9.7×10^{-4}	−1.8	5.5

[a] $\Delta\sigma^2$(model complex) ± 30%. [b] ΔE_0(model complex) ± 1.5 eV. [c] Fe–N ± 0.015 Å. [d] Fe–N ± 0.025 Å. [e] Fe–N ± 0.04 Å.

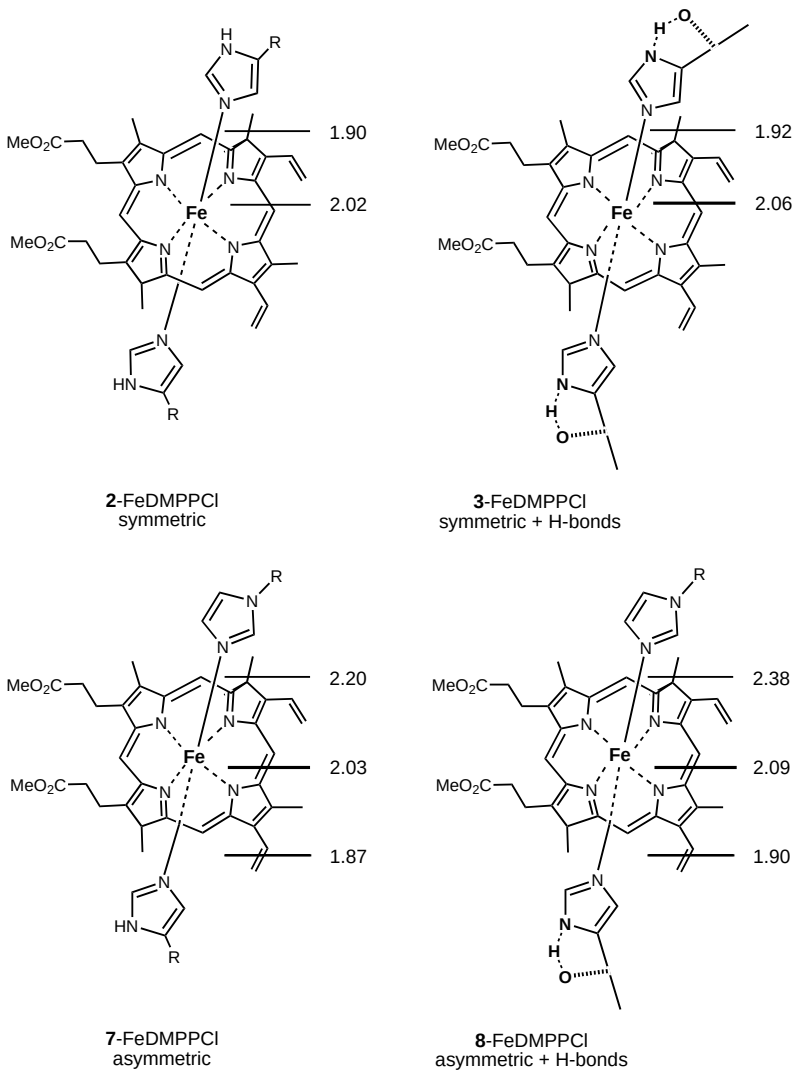

Scheme 3. Pictorial representation of the XAS results (Tables 2 and 4), reflecting the changes in the first coordination shell of the heme analogue FeDMPPCl due to complexation with four selected bis-imidazole ligands.

The Fe–*N*-alkyl imidazole bonds in complexes of ligands **8** or **9** with FeDMPPCl were found to be even weaker. In these complexes, hydrogen bonding at the NH imidazole side chain resulted in increased electron density on the Fe center that imposed additional elongation of the Fe–X bonds up to almost 2.40 Å, ≈0.5 Å longer than the axial bonds in **1**-FeDMPPCl. The Fe–N_{im} bond lengths in these complexes remained similar (≈1.90 Å), while the Fe–N_p bonds were elongated like those for H-bonding in complexes of the symmetric ligands, **3** and **6**. The blue shift in the UV/Vis spectrum of **9**-FeTPPCl, due to the nonsymmetric binding, was more significant than that observed in the spectrum of **7**-FeTPPCl. The Soret and Q-bands (406 nm, shifted by 12 nm or 525, shifted by 25 nm relative to **2**-FeTPPCl, respectively) are similar to those obtained with (six-coordinating) high-spin Fe^{III}-porphyrin complexes.

The results with complexes of ligands **8** and **9** show that nonsymmetry in the ligand head groups indeed produces 1:1

Table 4. Comparison of first-coordination-shell bond lengths in complexes of the nonsymmetric ligands (**7**–**9**),[a] and in the active site of peroxidases.[b][11]

bond	**7**-FeDMPPCl	**7**-FeTPPCl	**8**-FeDMPPCl	**9**-FeDMPPCl
Fe–N_p	2.03	2.01	2.09	2.05
Fe–N_{im}	1.87	1.91	1.90	1.81
Fe-X	2.20	2.14	2.38	2.26
	ARP	MPO	HRP	CcP
Fe–N_p	2.02	2.03	2.04	2.05
Fe–N_{im}	1.89	1.93	1.90	1.94
Fe-X	2.10	2.13	2.39	2.30

[a] Fe-N_p=Fe to N(pyrrole) average length ±0.015 Å, Fe-N_{im}=Fe to N(closer axial imidazole) length ±0.025 Å, Fe-X=Fe to N(longer axial imidazole or distal ligand) length ±0.04 Å. [b] ARP: *Arthromyces ramosus* peroxidase, MPO: myeloperoxidase, HRP: horseradish peroxidase, CcP: cytochrome C peroxidase.

complexes with nonsymmetric axial ligation to Fe^{III}. In addition, H-bonding within only one ligand arm increases the electron density at the Fe^{III} center; this elongates both the Fe–N_p bonds and that of the opposite axial ligand (Fe–X).

Comparison with the peroxidases: The electron density at the iron center in bis-imidazole hemes can be finely tuned by H-bonding and nonsymmetry in the axial ligands. These modifications are presented graphically in Scheme 3, which shows the first-coordination-shell bond lengths in four selected complexes, taken from Table 2 and Table 4. These demonstrate the design basis for novel peroxidase biomimetic compounds.

Table 4 compares the results for complexes of ligands **7**–**9** to the first coordination shells of native peroxidases. Note that the distal ligand in our complexes is always an *N*-alkyl imidazole, while in the peroxidases it is a water molecule or an amino acid side chain. The complexes **7**-FeTPPCl and **7**-FeDMPPCl are very similar to the first-coordination-shell bond lengths of *Arthromyces ramosus* peroxidase (ARP)[11] and myeloperoxidase (MPO).[48] In ARP, Asp246 is hydrogen bonded to the proximal histidine (His170), in MPO it is Asn421 (to His336).[15, 49] Complexes of **8** and **9** with FeDMPPCl, in which H-bonding caused a lengthening of the distal ligand bond and the average Fe–N_p lengths, are very similar to the active sites of horseradish peroxidase (HRP)[5, 11] and cytochrome C peroxidase (CcP).[5, 9, 11] Both HRP and CcP have hydrogen-bonding *networks* involving one or two hydrogen bonds to the aspartic acid (HRP: Asp247, CcP: Asp235), which in turn is hydrogen bonded to the proximal histidine.[50, 51] These hydrogen-bonding networks are probably stronger than the single H-bond of ARP and MPO.

It is interesting to note that the effect on the Fe^{III} electron density due to substitution of the porphyrin periphery by electron-withdrawing or -donating groups, which we and others[25] have observed, was also demonstrated in proteins by substitution at the 2- and 4-positions of the heme in HRP.[12] Increased electron density at the HRP heme resulted in lengthening of the Fe–N_p bonds, the same effect we saw in our models with complexes of FeTmPPCl (see Table 2). Thus, there are two alternative ways by which it is possible to control the electron density at iron–porphyrin active sites, either in heme proteins or model compounds.

Peroxidase activity: The reddish-brown solutions of **7**-FeTPPCl or **9**-FeTPPCl in DMF or CH_2Cl_2/CH_3OH turned green when the complexes were oxidized by *m*CPBA at low temperatures ($T < -20\,^{\circ}C$); this indicated the formation of ferryl radical cation species—analogues of the peroxidase compound **I**. Attempts to oxidize complexes of the symmetric ligands **2**-FeTPPCl and **3**-FeTPPCl under these conditions failed. The difference in behavior is probably due to the fact that in complexes of the nonsymmetric ligands one imidazole is bound weakly and was released to facilitate the introduction of the oxidative reagent. This explanation is supported by our observation that at lower temperatures (e.g. $-78\,^{\circ}C$) the complex was unreactive, unlike complexes with no axial ligands (e.g. $FeTMP^+$).[19] In order to characterize the reactive species that were formed by **7**-FeTPPCl and **9**-FeTPPCl, we followed their formation by optical absorption and ^1H NMR spectroscopy.

Addition of 5–10 equivalents of *m*CPBA to solutions of **7**-FeTPPCl or **9**-FeTPPCl ($1-5\times10^{-5}$ M, DMF, $25\,^{\circ}C$) in the optical absorption cells resulted in the appearance of a new spectrum (Figure 3) that was characterized by peaks at 554, 643, and 675 nm. This spectrum is very similar to the spectra of other oxo-ferryl radical cations of tetraphenyl iron–porphyrins.[19, 21, 52–54] Under these conditions, the radical cation was generated in 20 minutes and remained stable for another few minutes. The Soret band is only slightly shifted relative to the starting spectrum (418 nm); this suggests that one imidazole was still bound to the Fe center, although we could not eliminate the possibility that a DMF molecule had been coordinated.[21]

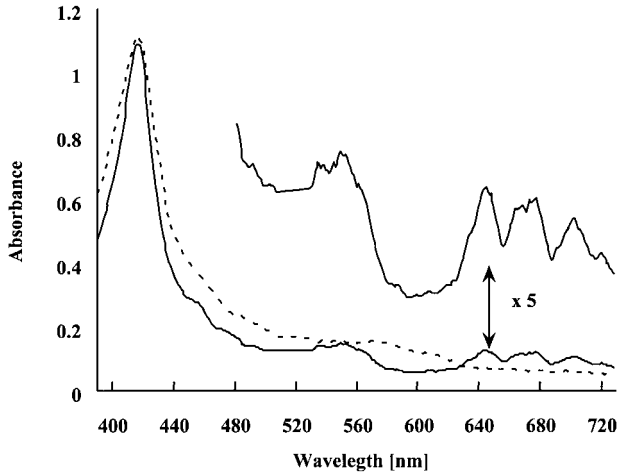

Figure 3. UV/Vis spectra of **7**-FeTPPCl, 2.5×10^{-5} M in DMF at $-25\,^{\circ}C$, before (----) and 20 minutes after (——) the addition of 10 mol equivalents of the oxidative reagent *m*CPBA.

EXAFS data analysis of the frozen intermediates indicated that the long axial ligand had been replaced by another ligand, probably an oxygen, having a bond length comparable to that of the hydrogen-bonded imidazole ligand (≈1.8 Å).[55] These results also indicate that the iron had been oxidized, as the

0947-6539/02/0817-4024 $ 20.00+.50/0 *Chem. Eur. J.* **2002**, *8*, No. 17

absorption edge was shifted by approximately 2 eV to higher energy.[5]

The oxidation of **7**-FeTPPCl by *m*CPBA was followed by ^{1}H NMR spectroscopy (5–10 mM, [D$_7$]DMF, $-33\,^\circ$C). The spectrum of the radical cation is characterized by a β-pyrrole peak at $\delta = 13.8$ ppm and by a broad *o*-phenyl peak centered at $\delta = -4.1$ ppm. These are very similar to the chemical shifts observed earlier for radical cations of Fe^{IV} tetrakis(*o*-pivalamidophenyl) porphyrin chloride.[53] Other peaks in the vicinity of the iron center could not be resolved because they overlapped those of the ligand. The low-spin chemical shifts of β-pyrrole ($\delta = -23.6$ ppm) and of CH$_2$-imidazolyls ($\delta =$ 17.9, 19.2 ppm) disappeared almost completely. Quenching of the reactive species back to the UV/Vis or ^{1}H NMR spectra of the low-spin complexes was done by elevating the temperature ($T > -5\,^\circ$C) or by the addition of cyclooctene as a substrate for further oxidation.

In order to further asses the reactivity of the various complexes, we used a modified version of the method that is utilized in ELISA applications to oxidize the chromogen ABTS by HRP and H_2O_2.[44, 56] Complexes **2**-, **7**- and **9**-FeTPPCl (1.3×10^{-5} M in DMF) catalyzed the oxidation of ABTS in DMF, with *m*CPBA as the oxidant. The optical absorption maxima of ABTS ($\approx$340 nm, split to three peaks) decreased upon addition of the oxidant to a mixture of each of the complexes with ABTS. The typical spectrum of the green ABTS radical cation with a maximum at 420 nm appeared.[44] Successive additions of *m*CPBA resulted in total conversion to the radical cation. The reactivity of the three complexes as catalyst for oxidation was compared, under identical conditions, by following the kinetics of the spectral changes during the initial steps of oxidation. Example values for k_2 to oxidize ABTS (3.1 equiv. with respect to the studied complex) after addition of *m*CPBA (80 equiv.) at room temperature (23 $^\circ$C) were as follows: $1.1 \times 10^4 \pm 1 \times 10^3\ s^{-1}$ for **2**-FeTPPCl ($t_{1/2} =$ 1.8 s), $3.2 \times 10^4 \pm 2 \times 10^3\ s^{-1}$ for **7**-FeTPPCl (0.6 s), and $4.1 \times 10^4 \pm 2 \times 10^3\ s^{-1}$ for **9**-FeTPPCl (0.4 s). The same trends were also observed if the reaction conditions, that is, temperature, concentration, or total volume, were varied. The most reactive was **9**-FeTPPCl, which is nonsymmetric and possesses H-bonds, while **7**-FeTPPCl, which lacks H-bonds, was less reactive. As expected from the above-described experiment to form the oxoferryl radical cation, **2**-FeTPPCl is a significantly less reactive catalyst.

Our current efforts focus on performing molecular-heterogeneous catalysis by using monolayers of the complexes on solid substrates. The preliminary solution studies showed that complexes of our ligands with MnTPPCl catalyze epoxidation and hydroxylation reactions with H_2O_2 as the oxidant.[57] The reactions in which the nonsymmetric complexes (**7**- and **9**-MnTPPCl) served as catalysts were faster and produced higher yields than reactions with the symmetric complexes (**1**- and **2**-MnTPPCl) or with imidazole complexes.

Conclusion

We have demonstrated that understanding the key structural features of an active site is sufficient to reproduce it by different chemical means. Therefore, our model system represents by definition a *biomimetic* approach to enzyme design. Gradual modifications in the structure of simple ligands lead to the conclusions that nonsymmetry in ligand head groups induces nonsymmetric axial ligation to Fe^{III} porphyrins, and that H-bonding within only one ligand arm expands the porphyrin core and elongate the opposite axial ligation. Due to the H-bonding, the electron density at the Fe^{III} center increases to facilitate the catalytic activity. These results mimic those observed previously for the peroxidase family. The methods described here, with simple ligands, can probably be used to mimic the nature of other metalloprotein families.

Acknowledgements

We thank Rachel Lazar and Urs Kropf for their help in the synthesis. A.S. holds the Siegfried and Irma Ullman Professorial Chair.

[1] B. Chance, *Arch. Biochem.* **1949**, *22*, 224–252.
[2] G. R. Schonbaum, S. Lo, *J. Biol. Chem.* **1972**, *247*, 3353–3360.
[3] P. George, D. H. Irvine, *Biochem. J.* **1952**, *52*, 511–517.
[4] N. K. King, M. E. Winfield, *J. Biol. Chem.* **1963**, *238*, 1520–1528.
[5] B. Chance, L. Powers, Y. Ching, T. Poulos, G. R. Schonbaum, Y. Yamazaki, G. K. Paul, *Arch. Biochem. Biophys.* **1984**, *235*, 596–611.
[6] M. Chance, L. Powers, C. Kumar, B. Chance, *Biochemistry* **1986**, *25*, 1259–1265.
[7] R. Sinclair, I. Yamazaki, J. Bumpus, B. Brock, C. S. Chang, A. Albo, L. Powers, *Biochemistry* **1992**, *31*, 4892–4900.
[8] R. Sinclair, B. Copeland, I. Yamazaki, L. Powers, *Biochemistry* **1995**, *34*, 738–740.
[9] R. Sinclair, S. Hallaman, M. Chen, B. Chance, L. Powers, *Biochemistry* **1996**, *35*, 15120–15128.
[10] C. S. Chang, R. Sinclair, S. Khalid, I. Yamazaki, S. Nakamura, L. Powers, *Biochemistry* **1993**, *32*, 2780–2786.
[11] L. Powers, *Molecular Electronics and Molecular Electronic Devices*, CRC Press, **1994**, pp. 211–223.
[12] B. He, R. Sinclair, B. R. Copeland, R. Makino, L. S. Powers, I. Yamazaki, *Biochemistry* **1996**, *35*, 2413–2420.
[13] B. Henrissat, M. Saloheimo, S. Lavaitte, J. K. C. Knowless, *Proteins: Struct. Funct. Genet.* **1990**, *8*, 251–257.
[14] T. Poulos, S. Edwards, H. Wariishi, M. Gold, *J. Biol. Chem.* **1993**, *268*, 4429–4440.
[15] N. Kunishima, K. Fukuyama, H. Matsubara, H. Hatanaka, Y. Shibano, T. Aamachi, *J. Mol. Biol.* **1994**, *235*, 331–337.
[16] R. Fenna, J. Zeng, C. Davey, *Arch. Biochem. Biophys.* **1995**, *316*, 653–656.
[17] D. Schuller, N. Ban, R. v. Huystee, A. McPherson, T. Poulos, *Structure* **1996**, *4*, 311–321.
[18] R. Quinn, J. Mercersmith, J. N. Burstyn, J. S. Valentine, *J. Am. Chem. Soc.* **1984**, *106*, 4136–4144.
[19] J. T. Groves, R. C. Haushalter, M. Nakamura, T. E. Nemo, B. J. Evans, *J. Am. Chem. Soc.* **1981**, *103*, 2884–2886.
[20] T. G. Traylor, W. A. Lee, D. V. Stynes, *J. Am. Chem. Soc.* **1984**, *106*, 755–764.
[21] A. Gold, K. Jayaraj, P. Doppelt, R. Weiss, G. Chottard, E. Bill, X. Ding, A. X. Trautwein, *J. Am. Chem. Soc.* **1988**, *110*, 5756–5761.
[22] P. Battioni, J. P. Renaud, J. F. Bartoli, M. Reina-Artiles, M. Fort, D. Mansuy, *J. Am. Chem. Soc.* **1988**, *110*, 8462–8470.
[23] M. W. Grinstaff, M. G. Hill, J. A. Labinger, H. B. Gray, *Science* **1994**, *264*, 1311–1313.
[24] D. Dolphin, T. G. Traylor, L. Y. Xie, *Acc. Chem. Res.* **1997**, *30*, 251–259.
[25] K. Yamaguchi, Y. Watanabe, I. Morishima, *J. Am. Chem. Soc* **1993**, *115*, 4058–4065.
[26] P. Obrien, D. A. Sweigart, *Inorg. Chem.* **1985**, *24*, 1405–1409.

  0947-6539/02/0817-4025 $ 20.00+.50/0

[27] N. Ueyama, N. Nishikawa, Y. Yamada, T. Okamura, A. Nakamura, *J. Am. Chem. Soc.* **1996**, *118*, 12826 – 12827.
[28] T. Ueno, Y. Kousumi, K. Yoshizawa-Kumagaye, K. Nakajima, N. Ueyama, T. Okamura, A. Nakamura, *J. Am. Chem. Soc.* **1998**, *120*, 12264 – 12273.
[29] C. Y. Yeh, C. J. Chang, D. G. Nocera, *J. Am. Chem. Soc.* **2001**, *123*, 1513 – 1514.
[30] D. G. Wu, G. Ashkenasy, D. Shvarts, R. V. Ussyshkin, R. Naaman, A. Shanzer, D. Cahen, *Angew. Chem.* **2000**, *112*, 4670 – 4674; *Angew. Chem. Int. Ed.* **2000**, *39*, 4496 – 4500.
[31] T. Moav, A. Hatzor, H. Cohen, J. Libman, A. Shanzer, I. Rubinstein, *Chem. Eur. J.* **1998**, *4*, 502 – 507.
[32] G. Ashkenasy, A. Ivanisevic, R. Cohen, C. E. Felder, D. Cahen, A. B. Ellis, A. Shanzer, *J. Am. Chem. Soc.* **2000**, *122*, 1116 – 1122.
[33] B. Chance, P. Angiolillo, E. Yang, L. Powers, *FEBS Lett.* **1980**, *112*, 178 – 182.
[34] M. Chance, L. Parkhurst, L. Powers, B. Chance, *J. Biol. Chem.* **1986**, *261*, 5689 – 5692.
[35] C. S. Chang, I. Yamazaki, R. Sinclair, S. Khalid, L. Powers, *Biochemistry* **1993**, *32*, 923 – 928.
[36] P. Lee, P. Citrin, P. Eisenberg, B. Kincaid, *Rev. Mod. Phys.* **1981**, *53*, 769 – 806.
[37] L. Powers, B. Kincaid, *Biochemistry* **1989**, *28*, 4461 – 4468.
[38] L. Powers, *Biochim. Biophys. Acta* **1982**, *683*, 1 – 38.
[39] L. Powers, J. Sessler, G. Woolery, B. Chance, *Biochemistry* **1984**, *23*, 239 – 244.
[40] B. Chance, R. Fischetti, L. Powers, *Biochemistry* **1983**, *22*, 3820 – 3829.
[41] E. Stern, B. Newville, B. Ravel, Y. Yacoby, D. Heskel, *Physica B* **1995**, *208 – 209*, 117 – 120.
[42] F. A. Walker, M.-W. Lo, M. T. Ree, *J. Am. Chem. Soc.* **1976**, *98*, 5552 – 5560.
[43] W. L. Zhu, H. L. Jiang, C. M. Puah, X. J. Tan, K. X. Chen, Y. Cao, R. Y. Ji, *J. Chem. Soc. Perkin Trans. 2* **1999**, *11*, 2615 – 2622.
[44] R. E. Childs, W. G. Bardsley, *Biochem. J.* **1975**, *145*, 93 – 103.
[45] G. La-Mar, J. Frye, J. Satterlee, *Biochim. Biophys. Acta* **1976**, *428*, 78 – 90.
[46] P. Yakirevitch, N. Rochel, A. Albrecht-Gary, J. Libman, A. Shanzer, *Inorg. Chem.* **1993**, *32*, 1779 – 1787.
[47] R. Quinn, C. E. Strouse, J. S. Valentine, *Inorg. Chem.* **1983**, *22*, 3934 – 3940.
[48] K. T. Yue, K. L. Taylor, J. M. J. Kinkade, R. B. Sinclair, L. S. Powers, *Biochim. Biophys. Acta* **1997**, *1338*, 282 – 294.
[49] J. Zeng, R. E. Fenna, *J. Mol. Biol.* **1992**, *226*, 185 – 190.
[50] B. C. Finzel, T. L. Poulos, J. Kraut, *J. Biol. Chem.* **1984**, *259*, 13027 – 13036.
[51] M. Gajhede, D. J. Schuller, A. Henriksen, A. T. Smith, T. L.Poulos, *Nat. Struct. Biol.* **1997**, *4*, 1032 – 1039.
[52] A. Gold, K. Jayaraj, P. Doppelt, R. Weiss, E. Bill, X. Q. Ding, E. L. Bominaar, A. X. Trautwein, H. Winkler, *New J. Chem.* **1989**, *13*, 169 – 172.
[53] D. Mandon, R. Weiss, M. Franke, E. Bill, A. X. Trautwein, *Angew. Chem.* **1989**, *101*, 1747 – 1750, *Angew. Chem. Int. Ed. Engl.* **1989**, *28*, 1709 – 1711.
[54] D. Mandon, R. Weiss, K. Jayaraj, A. Gold, J. Terner, E. Bill, A. X. Trautwein, *Inorg. Chem.* **1992**, *31*, 4404 – 4409.
[55] M. T. Green, *J. Am. Chem. Soc.* **2000**, *122*, 9495 – 9499.
[56] K. K. Makinen, J. Tenovou, *Anal. Biochem.* **1982**, *126*, 100 – 108.
[57] G. Ashkenasy, A. Shanzer, A. M. Khenkin, R. Neumann, unpublished results.

Received: July 20, 2001
Revised: May 2, 2002 [F3428]

  0947-6539/02/0817-4026 $ 20.00+.50/0